Least action description of dynamic pairing correlations in the fission of curium and californium isotopes based on the Gogny energy density functional

R. Rodríguez-Guzmán,[1,*] L. M. Robledo,[2,3,†] Carlos A. Jiménez-Hoyos,[4,‡] and N. C. Hernández[3,§]

[1]*Departamento de Física Aplicada I, Escuela Politécnica Superior, Universidad de Sevilla, Seville E-41011, Spain*

[2]*Center for Computational Simulation,Universidad Politécnica de Madrid, Campus Montegancedo, 28660 Boadilla del Monte, Madrid, Spain*

[3]*Departamento de Física Teórica and CIAFF, Universidad Autónoma de Madrid, 28049-Madrid, Spain*

[4]*Department of Chemistry, Wesleyan University, Middletown, Connecticut 06459, USA*

(Received 20 January 2023; accepted 28 March 2023; published 11 April 2023)

The impact of dynamic pairing correlations and their interplay with Coulomb antipairing effects on the systematic of the spontaneous fission half-lives for the nuclei $^{240-250}$Cm and $^{240-250}$Cf is analyzed, using a hierarchy of approximations based on the parametrization D1M of the Gogny energy density functional (EDF). First, the constrained Hartree-Fock-Bogoliubov (HFB) approximation is used to compute deformed mean-field configurations, zero-point quantum corrections and collective inertias either by using the Slater approximation to Coulomb exchange and neglecting Coulomb antipairing or by fully considering the exchange and pairing channels of the Coulomb interaction. Next, the properties of the *least action* and *least energy* fission paths are compared. In the *least action* case, pairing is identified as the relevant degree of freedom in order to minimize the action entering the Wentzel-Kramers-Brillouin (WKB) approximation to the tunneling probability through the fission barrier. Irrespective of the treatment of Coulomb exchange and antipairing, it is shown that the *least action* path obtained taking into account the pairing degree of freedom leads to stronger pairing correlations that significantly reduce the spontaneous fission half-lives $t_{\rm SF}$ improving thereby the comparison with the experiment by several orders of magnitude. It is also shown that the Coulomb antipairing effect is, to a large extent, washed out by the *least action* procedure and therefore the $t_{\rm SF}$ values obtained by the two different treatments of the Coulomb exchange and pairing are of similar quality.

DOI: 10.1103/PhysRevC.107.044307

I. INTRODUCTION

How to account for the most relevant correlations along different fission paths of atomic nuclei still represents a major challenge in modern nuclear structure physics [1,2]. Along its different fission paths, the nucleus exhibits pronounced shape changes consequence of the subtle balance between Coulomb, surface energy, and quantum shell effects associated with the underlying single-particle structure. Within the mean-field approximation [3] often used in nuclear physics to characterize nuclear dynamics, those shape changes are usually imposed with the help of constrains on certain operators $\hat{\mathbf{Q}}$ such as, for example, the quadrupole $\hat{Q}_{20}$ and $\hat{Q}_{22}$, axial octupole $\hat{Q}_{30}$, axial hexadecupole $\hat{Q}_{40}$ and necking $\hat{Q}_{\rm Neck}$ operators [1,4,5]. Microscopic mean-field studies of fission-related quantities are usually carried out using both nonrelativistic [4–22] and relativistic [23–29] energy density functionals (EDFs).

Many of the mean-field fission studies available in the literature make use of the *least energy* (LE) principle that imposes each $\mathbf{Q}$ configuration along the fission path to be determined by minimizing the mean-field energy. Short-range pairing correlations, of great importance for nuclear dynamics, are taken into account within the mean-field approach by introducing the Bogoliubov-Valatin canonical transformation to quasiparticles that leads to the Hartree-Fock-Bogoliubov (HFB) mean-field equations. As a consequence of the structure of the quasiparticle operators, particle number is not preserved at the mean-field level and the associated U(1) gauge symmetry is broken [3]. The amount of pairing correlations present in each configuration determines the size of the collective inertias associated with shape degrees of freedom and therefore have a strong influence in fission observables like spontaneous fission have-lives $t_{\rm SF}$ or fragment mass distributions. The LE scheme, based on several parametrizations of the Gogny-EDF [6], has been employed to study the fission properties of even-even Ra, U, Pu, and superheavy nuclei [4,14,30,31] as well as odd-mass U, Pu, and No nuclei [32,33] within the equal filling approximation (EFA) [34]. Those previous HFB studies [4,30–33] revealed that modifications of a few percent in the pairing strength of the interaction can have a significant impact on the collective masses, leading to uncertainties of several orders of magnitude in the predicted $t_{\rm SF}$ values.

The impact of dynamic (beyond-mean-field) pairing correlations on fission properties has been recently studied [35,36]

*raynerrobertorodriguez@gmail.com
†luis.robledo@uam.es
‡cjimenezhoyo@wesleyan.edu
§norge.us.es

using a LE restricted variation after particle number projection (RVAP-PNP) approach. A variational mean-field subspace has been built for each **Q** configuration along the fission path by using constraints on particle number fluctuation for both protons and neutrons separately. The optimal mean-field state is then determined by searching for the minimum of the particle-number-projected energy in this subspace. The main outcome of the first study mentioned before was that the increase of pairing correlations associated with RVAP-PNP is compensated by its quenching due to Coulomb antipairing and the final results are very similar to those of the mean-field. At this point it is worth recalling that Coulomb antipairing is neglected in mean-field studies but it has to be fully taken into account in the PNP procedure to avoid the Pauli principle violation problem of symmetry restoration [37]. A later study [36] revealed that, for nuclei with low and narrow fission barriers, the compensation between Coulomb antipairing and beyond-mean-field pairing effects might not be perfect leading to a modulation of the $t_{\rm SF}$ values, as functions of the neutron number, due to PNP. Thus, for such nuclei, the combined Coulomb antipairing and LE RVAP-PNP effects cannot be overlooked, neither can they be accounted for by the Coulomb Slater approximation [38].

Dynamic pairing correlations, have also been studied within the *least action* (LA) principle. Here, at variance with the LE scheme, each configuration along the fission path is determined by the minimum of the action $\mathcal{S}$ written in terms of a set of selected collective variables. The motivation for the use of the LA principle is that the transmission probability through the fission barrier is proportional to the exponential of the action. It is well known in the literature [39,40] that the LE and LA schemes provide similar results when only shape constrains are considered. However, the situation is rather different when pairing degrees of freedom are taken into account in the minimization of the action [40,41]. In this case, the competition between the rapid changes in the collective inertia (decreasing as the inverse of the pairing gap [42,43]) and the energy (increasing as the square of the pairing gap) leads to a minimum of the action $\mathcal{S}$ for a pairing gap far larger than the one corresponding to the minimum-energy configuration. The value of the action at the minimum is much smaller than its value at the minimum-energy configuration. It is precisely this reduction of the action that leads to a decrease of the predicted LA half-lives as compared with the LE ones [39–41,44–50] bringing them in closer agreement with experimental data. Furthermore, the well-known dispersion in the predicted $t_{\rm SF}$ values arising from the use of the generator coordinate method (GCM) and/or adiabatic time-dependent HFB (ATDHFB) masses [4] is significantly reduced [41] within the LA scheme. It has also been shown that LA pairing fluctuations can restore axial symmetry along the fission path [47,51].

The results already mentioned clearly point towards the need for better understanding the impact of LA pairing correlations in fission calculations, especially in those cases where calculations are based on sophisticated microscopic Gogny and/or Skyrme EDFs. Such correlations have already been considered in previous LA Gogny-EDF studies [40,41]. Nevertheless, in all those calculations, the Coulomb exchange term has been considered in the Slater approximation [38] while Coulomb and spin-orbit antipairing are neglected (this approximation will be referred to hereafter as CESlater).

In this paper, we extend our previous LA studies [40,41] to a set of Cm and Cf nuclei for which experimental data are available [52]. The selected nuclei, i.e., $^{240-250}$Cm and $^{240-250}$Cf belong to a region of the nuclear chart where several key features of the shell effects associated with superheavy elements start to manifest [14,32]. One goal of this work is to examine the role of pairing correlations in the LA framework for such nuclei using the CESlater approximation. Our second and most relevant goal is to examine the interplay between Coulomb antipairing effects and dynamic pairing correlations within the LA scheme. To this end, calculations have been carried out including all the direct, exchange, and pairing contributions coming from the Gogny-EDF [6]. In particular, the Coulomb exchange and pairing terms are treated exactly (this approximation will be referred to hereafter as CEE).

The quenching of pairing correlations due to the Coulomb interaction (Coulomb antipairing) is usually neglected due to the computational effort associated with the evaluation of Coulomb's pairing field. However, Coulomb antipairing effects lead to a severe reduction of the pairing gap [35,36,53,54] and therefore collective inertias will increase when this contribution is included, leading to an increase of the collective action and larger $t_{\rm SF}$ values. On the other hand, dynamic pairing correlations tend to increase the pairing gap reducing thereby the inertias, leading to a decrease of the action and smaller $t_{\rm SF}$ values. The combined effect of Coulomb antipairing and dynamic pairing correlations has already been considered within the LE RVAP-PNP approach [35,36]. In the present study, however, we consider the interplay between Coulomb antipairing and dynamic pairing correlations using a LA perspective. To the best of our knowledge, at least in the case of Gogny-like EDFs, the CSlater LA results discussed in this paper are the first of their kind reported in the literature for $^{240-250}$Cm and $^{240-250}$Cf. Furthermore, ours is the first systematic study of the interplay between Coulomb antipairing and dynamic pairing effects within the CEE LA framework.

The results discussed in this paper have been obtained with the parametrization D1M [55] of the Gogny-EDF [6]. The Gogny force has been chosen because its central part is finite range and this guarantees a consistent treatment of long-range and pairing correlations within the same framework. The parametrization D1M has already been shown to account reasonably well for fission-related properties in previous studies (see, for example, Refs. [6,30–33,40,41,55]). This is the reason driving its choice as a reference in the present study. However, in order to examine the robustness of the results with respect to the underlying Gogny-EDF, calculations have also been carried out with the D1S [6] and D1M* [56] parametrizations. The predicted D1S and D1M* trends are rather similar to those obtained with the Gogny-D1M EDF. Therefore, only Gogny-D1M results will be discussed in detail in this paper.

The paper is organized as follows: The methodology employed in this study is briefly outlined in Sec. II. In particular, in this section we outline the LE and LA schemes employed to compute the paths and spontaneous fission half-lives for the considered nuclei at the CESlater and CEE levels. The results

of our calculations are discussed in Sec. III. First, in Sec. III A, we illustrate the employed methodology in the case of ^{248}Cf. The systematic of the fission paths and spontaneous fission half-lives, obtained with each of the considered approaches, is discussed in Sec. III B for $^{240-250}$Cm and $^{240-250}$Cf. Finally, Sec. IV is devoted to the concluding remarks.

II. THEORETICAL FRAMEWORK

In this section, we briefly outline the methodology employed in this study [4,36,41] to obtain LE and LA fission paths as well as other fission-related quantities—see Refs. [4,36,41] for a more detailed account.

The starting point in all our considerations is the HFB mean-field method implemented for the finite range Gogny force [55]. Aside from the usual HFB constrains on both the proton $\hat{Z}$ and neutron $\hat{N}$ number operators [3], constrains on the mean value of the (axially symmetric) quadrupole $\hat{Q}_{20}$ and octupole $\hat{Q}_{30}$ operators have been employed to obtain the CESlater and/or CEE LE (static) paths. The mean values of other shape parameters like the hexadecupole $\hat{Q}_{40}$ and higher multipolarity operators are given by the Ritz-variational procedure [3] that determines each of the configurations along the LE paths. Parity is allowed to be broken at any stage of the calculations and a constrain on the operator $\hat{Q}_{10}$ is employed to prevent spurious effects associated with the center-of-mass motion [4].

We are aware of the role of triaxiality around the top of the static inner barriers (see, for example, Refs. [4,7,23]). However, it has also been found [19,27] that the lowering of the inner barrier, due to triaxiality, comes together with an increase in the collective inertia that tends to compensate in the calculation of the action. This result suggests that the axially symmetric path would be the preferred one in fission dynamics. Moreover, it has also been shown that pairing fluctuations can restore axial symmetry along the fission path [47,51]. Therefore, the impact of triaxiality in the spontaneous fission half-lives seems to be very limited and is not been considered in this study.

A constraint on the (total) particle number fluctuation operator $\Delta\hat{N}^2$ has also been added to obtain the CESlater and/or CEE LA paths (see below). In principle, constrains on both the proton and neutron number fluctuation operator should be considered separately [35,36,50]. However, as in previous Gogny-like calculations [40,41] and in order to alleviate the already substantial computational effort, especially at the CEE level, we have restricted to a constraint on the total particle number fluctuation operator. Nevertheless, we have also checked that considering a separate constraint on particle number fluctuations for protons and neutrons does not bring much as compared with the variation of the total particle number fluctuation.

The HFB quasiparticle creation and annihilation operators have been expanded in an axially symmetric (deformed) harmonic oscillator (HO) basis containing states with J_z quantum numbers up to $35/2$ and up to 26 quanta in the z direction. The basis quantum numbers are restricted by the condition

$$2n_\perp + |m| + q\, n_z \leqslant M_{z,\mathrm{MAX}}, \tag{1}$$

with $M_{z,\mathrm{MAX}} = 17$ and $q = 1.5$. This choice is well suited for the elongated prolate shapes typical of the fission process [4]. In addition, we have optimized the HO length parameters for each value of the quadrupole moment as to minimize the HFB energy. An approximate second-order gradient method has been used for the solution of the HFB equation [57] because it provides a fast and robust convergence to the HFB solution.

Within the Wentzel-Kramers-Brillouin (WKB) formalism the LE and LA spontaneous fission half-life t_{SF} (in seconds) has been computed [4,5,41] following the standard approach

$$t_{\mathrm{SF}} = 2.86 \times 10^{-21}(1 + e^{2\mathcal{S}}), \tag{2}$$

where the action $\mathcal{S}$ along the (one-dimensional Q_{20}-projected) fission path is the integral

$$S = \int_a^b dQ_{20}\mathcal{S}(Q_{20}) \tag{3}$$

between the classical turning points a and b of the action $\mathcal{S}(Q_{20})$ for each quadrupole moment

$$\mathcal{S}(Q_{20}) = \sqrt{2B(Q_{20})[V(Q_{20}) - (E_{\mathrm{min}} + E_0)]}. \tag{4}$$

In Eq. (3), the integration limits a and b represent classical turning points [42] for the potential $V(Q_{20})$ corresponding to the energy $E_{\mathrm{min}} + E_0$. The energy E_{min} corresponds to the absolute minimum of the considered path, while E_0 accounts for the true ground-state energy once quadrupole fluctuations are taken into account. Although E_0 could be obtained from the curvature and collective inertia around the ground-state minimum we have taken in this work the typical value $E_0 =$ 0.5 MeV for all the isotopes considered. We have checked that other values of E_0 [4], including those estimated in terms of the curvature of the fission path around the ground state and the ground-state collective quadrupole inertia [31], do not alter the qualitative conclusions of the present study.

From its definition (2), it is clear that the spontaneous fission half-life depends on the different approximations considered in the calculation as they impact the potential-energy surfaces and collective inertias. It is worth to remark that the collective potential $V(Q_{20})$ in Eq. (4) is given by the HFB(CESlater) and/or HFB(CEE) energies corrected by the corresponding quantum zero-point vibrational and rotational energies

$$V(Q_{20}) = E_{\mathrm{HFB}}(Q_{20}) - \Delta E_{\mathrm{rot}}(Q_{20}) - \Delta E_{\mathrm{vib}}(Q_{20}). \tag{5}$$

The collective mass $B(Q_{20})$ as well as the zero-point vibrational energy correction $\Delta E_{\mathrm{vib}}(Q_{20})$ have been computed using both the ATDHFB and GCM approaches. In all the computations of the t_{SF} values, the wiggles in the collective masses have been softened by means of a three point filter [4]. The rotational energy correction $\Delta E_{\mathrm{rot}}(Q_{20})$ has been computed in terms of the Yoccoz moment of inertia [1,3,4,41,58,59].

In what follows, we outline the methodology employed to obtain the (CESlater and CEE) LE and LA fission paths. First, (Q_{20}, Q_{30})-constrained HFB(CESlater) calculations have been carried out for each of the considered nuclei. The two HO length parameters b_z and $b_\perp$ characterizing the HO basis have been optimized so as to minimize the total mean-field energy for each configuration along the LE

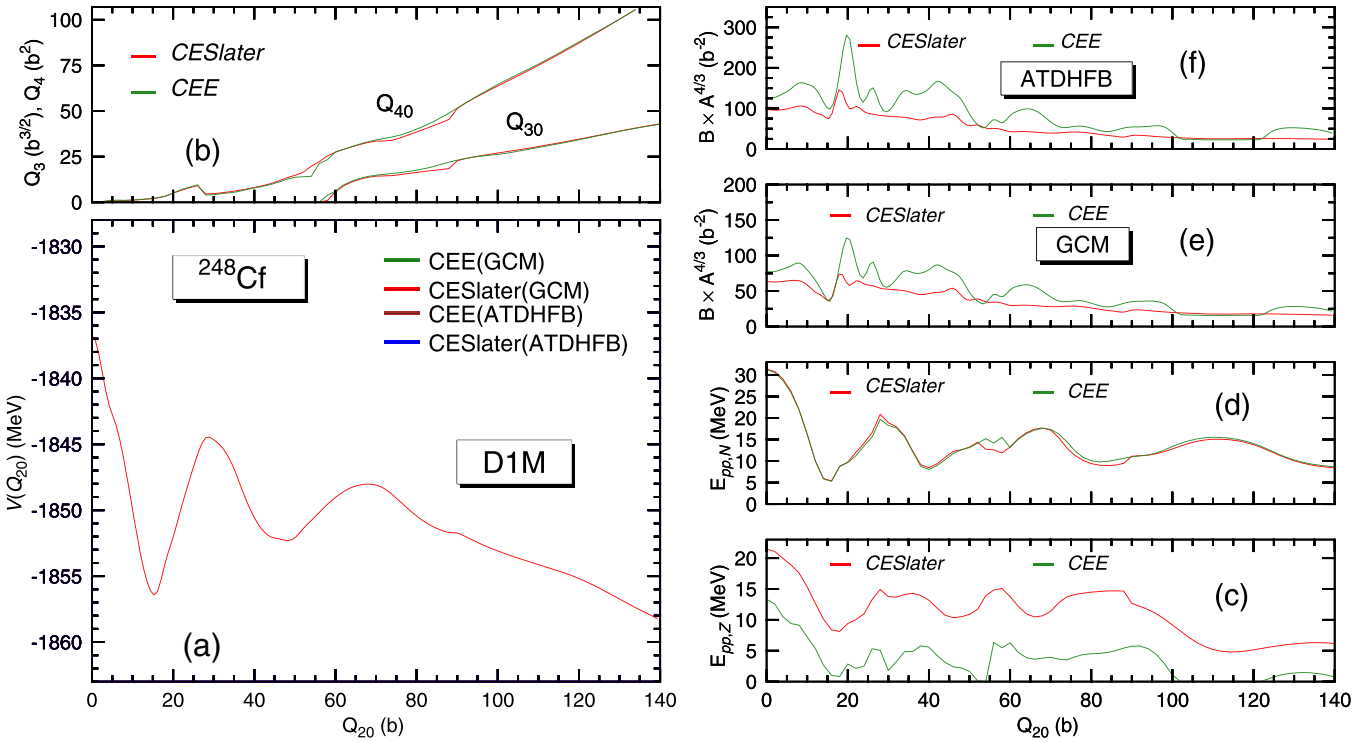

FIG. 1. The CESlater and CEE *least energy* (LE) collective potentials $V(Q_{20})$ (5) obtained for the nucleus ^{248}Cf, within the GCM and ATDHFB schemes, are plotted in panel (a) as functions of the quadrupole moment Q_{20}. The octupole Q_{30} and hexadecupole Q_{40} moments of the intrinsic states are plotted in panel (b). The proton $E_{pp,Z}$ and neutron $E_{pp,N}$ pairing interaction energies are depicted in panels (c) and (d), while the collective GCM and ATDHFB masses are plotted in panels (e) and (f). Results have been obtained with the parametrization D1M of the Gogny-EDF.

fission path [4]. Using the HFB(CESlater) wave functions as starting input, (Q_{20}, Q_{30})-constrained HFB(CEE) calculations have then been carried out for $^{240–250}$Cm and $^{240–250}$Cf without further optimizing the lengths of the HO basis to alleviate the computational effort. Zero-point quantum rotational and vibrational energies have been added *a posteriori* to the HFB(CESlater) and HFB(CEE) energies to obtain the collective potentials $V(Q_{20})$ according to Eq. (5). As illustrative examples, the CESlater and CEE LE collective potentials $V(Q_{20})$ obtained for the nucleus ^{248}Cf, within the GCM and ATDHFB schemes, are plotted in of Fig. 1(a) as functions of the quadrupole moment Q_{20}. The CESlater and CEE LA paths [40,41] considered in this paper are determined in the following way: for each Q_{20}-configuration along the CESlater and CEE LE paths, $(Q_{20}, \Delta N^2)$-constrained HFB(CESlater) and HFB(CEE) calculations are performed keeping constant the Q_{20} value and equal to the self-consistent solution of the LE path. The range of values of the constrained $\langle\Delta\hat{N}^2\rangle$ quantity starts at the self-consistent $\langle\Delta\hat{N}^2\rangle_{\rm self}$ value and extends until a minimum in the corresponding CESlater and CEE actions S is reached. We have used a small step size and, once more to alleviate the computational effort especially at the CEE level, we have optimized as much as possible the number of $\langle\Delta\hat{N}^2\rangle$ values required to reach a minimum of the action. Note, that at the CESlater and CEE level, the minimization is carried out for both the actions obtained using GCM and ATDHFB inertias, i.e., two CESlater and CEE dynamic paths are determined [41].

III. DISCUSSION OF THE RESULTS

The methodology employed for all the nuclei considered in this work is illustrated in the case of ^{248}Cf and described in detail in Sec. III A below. The systematic of the fission paths and spontaneous fission half-lives, obtained with each of the considered approaches, is discussed in Sec. III B for $^{240–250}$Cm and $^{240–250}$Cf.

A. An illustrative example: The nucleus ^{248}Cf

The CESlater and CEE LE collective potentials $V(Q_{20})$ (5) obtained for the nucleus ^{248}Cf, within the GCM and ATDHFB schemes, are plotted in Fig. 1(a) as functions of the quadrupole moment Q_{20}. The absolute minimum of the LE paths is located at $Q_{20} = 16$ b and is reflection symmetric ($Q_{30} = 0$). The fission isomer at $Q_{20} = 48$ b is separated from the ground state by the inner barrier, the top of which is located at $Q_{20} = 26$–28 b. Octupole correlations play a prominent role for quadrupole deformations $Q_{20} \geqslant 56$ b and significantly affect the height of the outer barrier, the top of which is located at $Q_{20} = 68$ b. For large quadrupole moments ($Q_{20} \geqslant 100$ b) the CEE LE collective potentials exhibit a faster decline than the CESlater ones [36]. The CESlater and CEE LE heights $B_{I,LE}$ and $B_{II,LE}$, computed within both the GCM and ATDHFB schemes, are given in Table I. The octupole Q_{30} and hexadecupole Q_{40} moments of the intrinsic states, depicted in Fig. 1(b), are rather similar in the CESlater and CEE approximations.

TABLE I. Heights, in MeV, of the inner (B_I) and outer (B_{II}) fission barriers obtained within the *least energy* (LE) and *least action* (LA) GCM and ATDHFB schemes for ^{248}Cf. Results are shown for the CESlater and CEE approaches with the Gogny-D1M EDF. The labels A and B correspond to the GCM and ATDHFB LE paths, whereas labels C and D are for the GCM and ATDHFB LA paths, respectively. For details, see the main text.

	$B_{I,A}$	$B_{II,A}$	$B_{I,B}$	$B_{II,B}$	$B_{I,C}$	$B_{II,C}$	$B_{I,D}$	$B_{II,D}$
CESlater	11.74	8.23	11.05	7.40	16.70	11.15	18.17	10.94
CEE	12.67	8.73	11.72	7.60	19.81	12.76	20.72	12.07

The HFB(CESlater) and HFB(CEE) proton and neutron pairing interaction energies [3] $E_{pp,\tau} = \frac{1}{2}\mathrm{Tr}(\Delta_\tau \kappa_\tau)$ (with $\tau = Z$ and N) are plotted in Figs. 1(c) and 1(d). As can be seen from Fig. 1(c), Coulomb antipairing effect severely quenches the proton pairing energies in the HFB(CEE) states as compared with the corresponding HFB(CESlater) values. On the other hand, as can be seen from Fig. 1(d), the HFB(CESlater) and HFB(CEE) neutron pairing energies are, as expected, rather similar.

The collective GCM and ATDHFB masses are plotted in Figs. 1(e) and 1(f). Both masses display a similar trend but the ATDHFB masses are, on the average, larger than the GCM ones [4,30–33,41]. This is the reason to consider both kinds of collective inertias in this work in the calculation of the corresponding LE and LA spontaneous fission half-lives. Regardless of the considered GCM and/or ATDHFB scheme, the HFB(CEE) collective inertia is larger than the HFB(CESlater) inertia and exhibits pronounced high peaks. This is a consequence of the quenching of proton pairing correlations in the HFB(CEE) solutions [see Fig. 1(c)] and the inverse dependence of the inertia with the square of the pairing gap [43].

The values of the spontaneous fission half-lives obtained in the LE scheme with both CESlater and CEE approaches are given in Table II for $E_0 = 0.5$ MeV. The $t^{\mathrm{ATDHFB}}_{\mathrm{SF,LE}}$ values are larger than the $t^{\mathrm{GCM}}_{\mathrm{SF,LE}}$ ones due to the differences in the corresponding collective inertias. Note that in both the GCM and ATDHFB schemes the increase observed in the HFB(CEE) collective inertias, due to Coulomb antipairing, leads to a pronounced increase in the spontaneous fission half-lives.

The CESlater and CEE LA collective potentials $V(Q_{20})$ (5) obtained for the nucleus ^{248}Cf, within the GCM and ATDHFB schemes, are plotted in Figs. 2(a) and 2(b) as functions of the quadrupole moment Q_{20}. The CESlater and CEE LE collective potentials are also included in the plots for comparison. The deformations of the absolute minimum, the top of the inner and outer barriers and the fission isomer in the dynamic paths are similar to those obtained for the static paths. In the case of the LA paths, octupole correlations play a key role for $Q_{20} \geqslant 54$ b.

As can be seen from Figs. 2(a) and 2(b), the most pronounced differences between the LA and LE paths appear around the spherical configuration as well as around the tops of the inner and outer barriers. This agrees with results obtained in previous Gogny LA calculations [40,41]. This is also in line with previous results obtained by the Warsaw-Lublin group (see, for example, the top panel of Fig. 1 in Ref. [50]) albeit with a simpler microscopic model. For example, at the CESlater level the spherical configuration lies 19.52 and 19.00 MeV above the LE GCM and ATDHFB absolute minima,

TABLE II. LE and LA spontaneous fission half-lives (in seconds) obtained with the GCM and ATDHFB collective inertias ($E_0 = 0.5$ MeV) for ^{248}Cf. Results are shown for the CESlater and CEE approaches with the Gogny-D1M EDF. The labels A and B correspond to the LE case with the GCM and ATDHFB inertias, whereas labels C and D are for the LA case with the GCM and ATDHFB inertias, respectively. For details, see the main text.

	$\log_{10} t_{\mathrm{SF,A}}$	$\log_{10} t_{\mathrm{SF,B}}$	$\log_{10} t_{\mathrm{SF,C}}$	$\log_{10} t_{\mathrm{SF,D}}$
CESlater	21.31	25.82	10.57	12.42
CEE	29.01	36.73	13.90	14.40

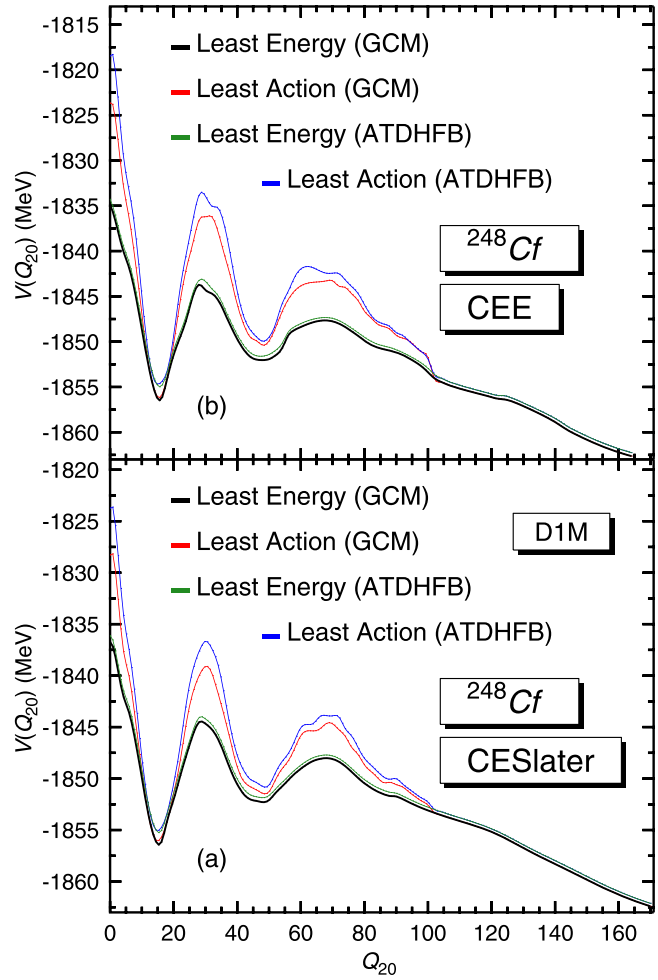

FIG. 2. The CESlater and CEE *least action* (LA) collective potentials $V(Q_{20})$ (5) obtained for the nucleus ^{248}Cf, within the GCM and ATDHFB schemes, are plotted in panels (a) and (b), as functions of the quadrupole moment Q_{20}. The CESlater and CEE *least energy* (LE) collective potentials are also included in the plots. Results have been obtained with the parametrization D1M of the Gogny-EDF. For more details, see the main text.

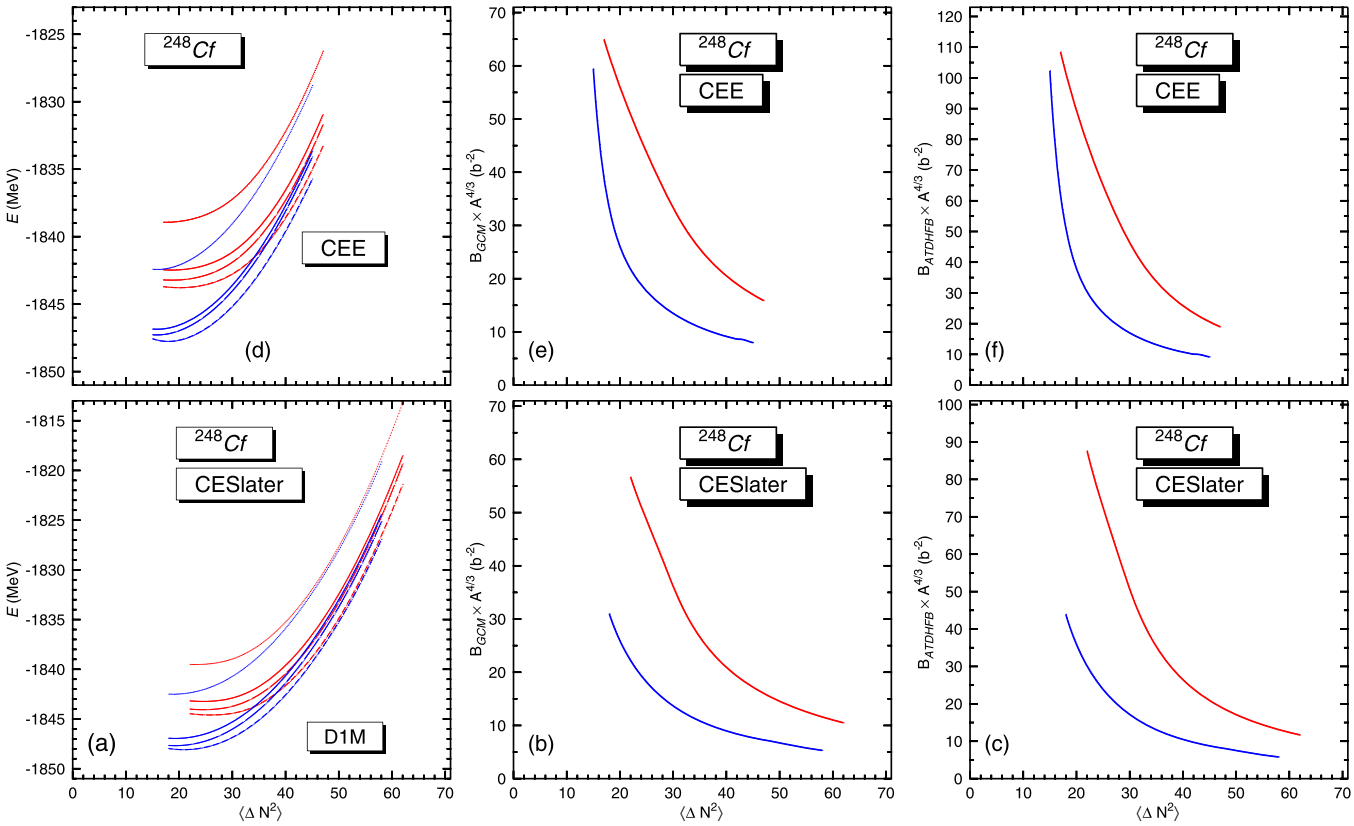

FIG. 3. The intrinsic HFB(CESlater) (full thin lines) [HFB(CEE) (full thin lines)], the HFB(CESlater) plus rotational correction energies (full thick lines) [HFB(CEE) plus rotational correction energies (full thick lines)], the HFB(CESlater) plus rotational and vibrational GCM correction energies (short dashed lines) [HFB(CEE) plus rotational and vibrational GCM correction energies (short dashed lines)] and the HFB(CESlater) plus rotational and vibrational ATDHFB correction energies (long dashed lines) [HFB(CEE) plus rotational and vibrational ATDHFB correction energies (long dashed lines)] are plotted in panel (a) [panel (d)] as functions of $\langle \Delta \hat{N}^2 \rangle$. The CESlater (CEE) GCM, and ATDHFB masses are depicted in panels (b) and (c) [(e) and (f)]. Results are shown for the quadrupole moments $Q_{20} = 28$ b (red) and 68 b (blue). For details, see the main text.

whereas it lies 27.52 and 31.09 MeV above the LA GCM and ATDHFB absolute minima. On the other hand, at the CEE level the spherical configuration lies 21.47 and 20.64 MeV above the LE GCM and ATDHFB absolute minima, whereas it lies 32.39 and 36.05 MeV above the LA GCM and ATDHFB absolute minima.

The LA GCM and ATDHFB heights of the inner and outer barriers, obtained at the CESlater and CEE levels, are also included in Table I for ^{248}Cf. The comparison between the LA and LE values given in the table, indicates that the former are always larger than the latter. This comparison should be done with care as the LE and LA values come from different approximations. On the one hand, contrary to cross sections, fission barriers are not experimental observables. Fission barriers (in particular, LE fission barriers) are usually inferred from cross sections using certain model assumptions. One of this assumptions relates with the particular form of the collective inertia considered. Within this context, the big differences in the table already raise the question about the suitability of a direct comparison between LE barrier heights and the experimentally determined ones (see also Ref. [60] and references therein) since, the role and behavior of the collective inertia should also be taken into account. We will come back to this point later on in the paper.

As already mentioned, our goal within the LA scheme is to minimize the action (3). To this end (see Sec. II), $(Q_{20}, \Delta N^2)$-constrained HFB(CESlater) and HFB(CEE) calculations have been performed, for each Q_{20} configuration along the LE CESlater and CEE fission paths of ^{248}Cf. In those calculations, we have always started at the self-consistent value $\langle \Delta \hat{N}^2 \rangle_{\rm self}$ for each Q_{20} deformation. However, in order to illustrate the inner workings of the LA scheme, it is also useful to examine the behavior of energies, collective masses and the integrand $\mathcal{S}(Q_{20})$ (4) of the action $\mathcal{S}$ (3) as functions of $\langle \Delta \hat{N}^2 \rangle$ [41]. Those quantities are plotted in Figs. 3 and 4 for quadrupole deformations $Q_{20} = 28$ and 68 b corresponding to the top of the inner and outer barriers, respectively.

The intrinsic HFB(CESlater) energies, the HFB(CESlater) plus rotational correction energies, the HFB(CESlater) plus rotational and vibrational GCM correction energies and the HFB(CESlater) plus rotational and vibrational ATDHFB correction energies are plotted in of Fig. 3(a). The CEE energies are shown in Fig. 3(d). For each of the considered Q_{20} values all those energies, i.e., the intrinsic and those including

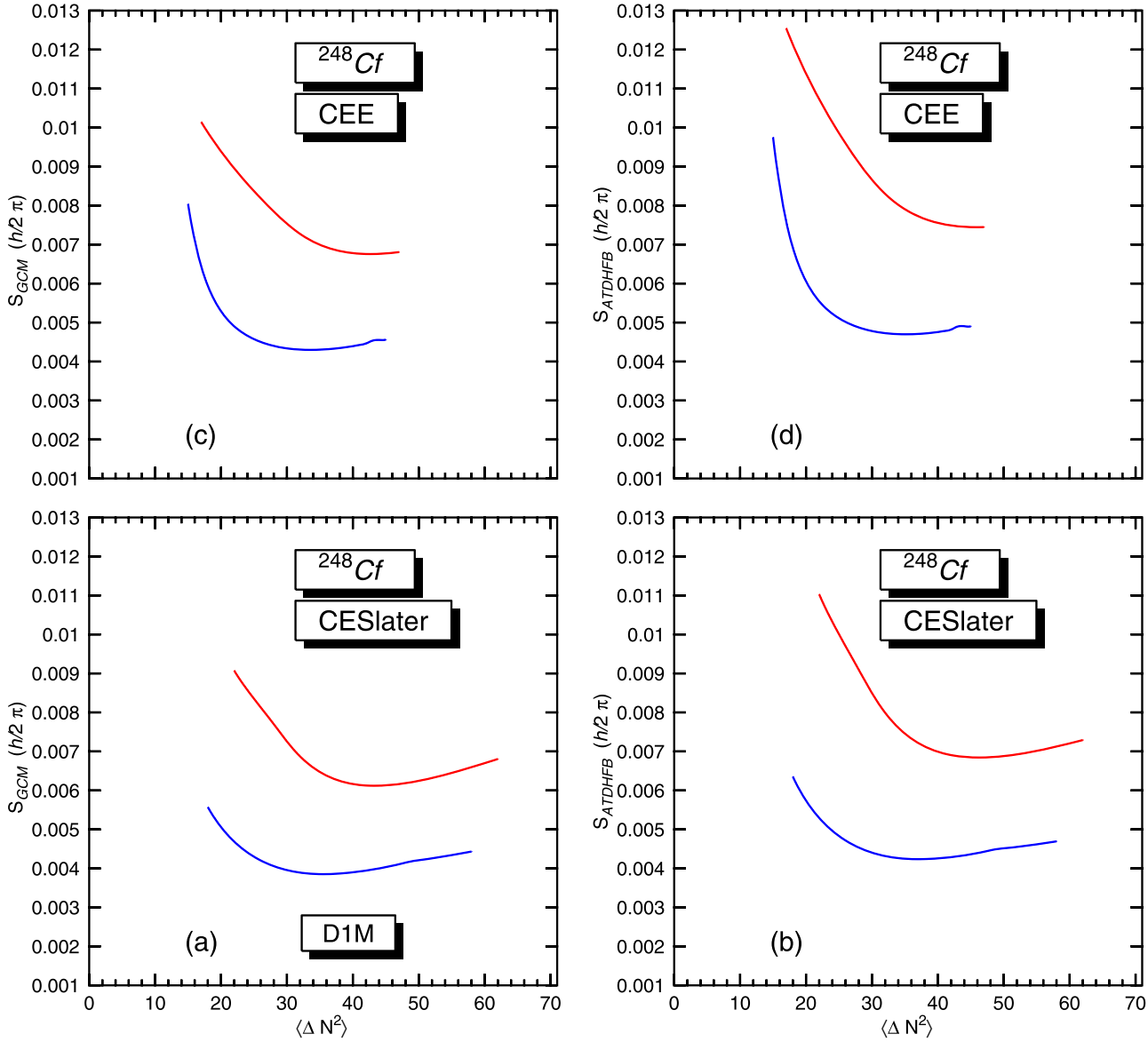

FIG. 4. The GCM and ATDHFB integrand (4) of the action (3) corresponding to the CESlater (CEE) approach are depicted in panels (a) and (b) [(c) and (d)] as functions of $\langle\Delta\hat{N}^2\rangle$. Results are shown for the quadrupole moments $Q_{20} = 28$ b (red) and 68 b (blue). For details, see the main text.

zero-point quantum fluctuations, exhibit an almost quadratic behavior as functions of $\langle\Delta\hat{N}^2\rangle$ with a minimum at $\langle\Delta\hat{N}^2\rangle = \langle\Delta\hat{N}^2\rangle_{\rm self}$.

The CESlater GCM and ATDHFB masses are depicted in Figs. 3(b) and 3(c), while the CEE masses are depicted in Figs. 3(e) and 3(f). Regardless of the differences in size, the collective masses always decrease for increasing $\langle\Delta\hat{N}^2\rangle$ values, reflecting their inverse dependence on the square of the pairing gap discussed in Refs. [42,43].

The CESlater GCM and ATDHFB integrands $\mathcal{S}(Q_{20})$ of the action $\mathcal{S}$ are shown in Figs. 4(a) and 4(b), while the corresponding CEE quantities are plotted in Figs. 4(c) and 4(d), respectively. The panels clearly illustrate the main mechanism at play within the LA framework, i.e., the competition between the increase of energies [Figs. 3(a) and 3(d)] and the decrease of the collective masses [Figs. 3(b), 3(c), 3(e), and 3(f)] as functions of $\langle\Delta\hat{N}^2\rangle$, leads to a minimum of the CESlater and CEE integrand $\mathcal{S}(Q_{20})$ for a $\langle\Delta\hat{N}^2\rangle$ value larger than $\langle\Delta\hat{N}^2\rangle_{\rm self}$. Moreover, as expected, the value of the integrand $\mathcal{S}(Q_{20})$ at the minimum is smaller than the one at $\langle\Delta\hat{N}^2\rangle_{\rm self}$. As an example, for the configuration at the top of the inner barrier ($Q_{20} = 28$ b) we have $\langle\Delta\hat{N}^2\rangle_{\rm self,CESlater} = 22$ which gives $\mathcal{S}_{\rm GCM,CESlater}(Q_{20} = 28b) = 9.07 \times 10^{-3}\hbar$ and $\mathcal{S}_{\rm ATD,CESlater}(Q_{20} = 28b) = 11.03 \times 10^{-3}\hbar$. On the other hand, $\mathcal{S}^{\rm min}_{\rm GCM,CESlater}(Q_{20} = 28b)$ [$\mathcal{S}^{\rm min}_{\rm ATD,CESlater}(Q_{20} = 28b)$] reaches a minimum value of $6.12 \times 10^{-3}\hbar$ ($6.84 \times 10^{-3}\hbar$) at $\langle\Delta\hat{N}^2\rangle = 43$ (46). Similar results are obtained at the CEE level. Here, for $\langle\Delta\hat{N}^2\rangle_{\rm self,CEE} = 17$, one obtains $\mathcal{S}_{\rm GCM,CEE}(Q_{20} = 28b) = 10.14 \times 10^{-3}\hbar$ and $\mathcal{S}_{\rm ATD,CEE}(Q_{20} = 28b) = 12.55 \times 10^{-3}\hbar$. The values at the

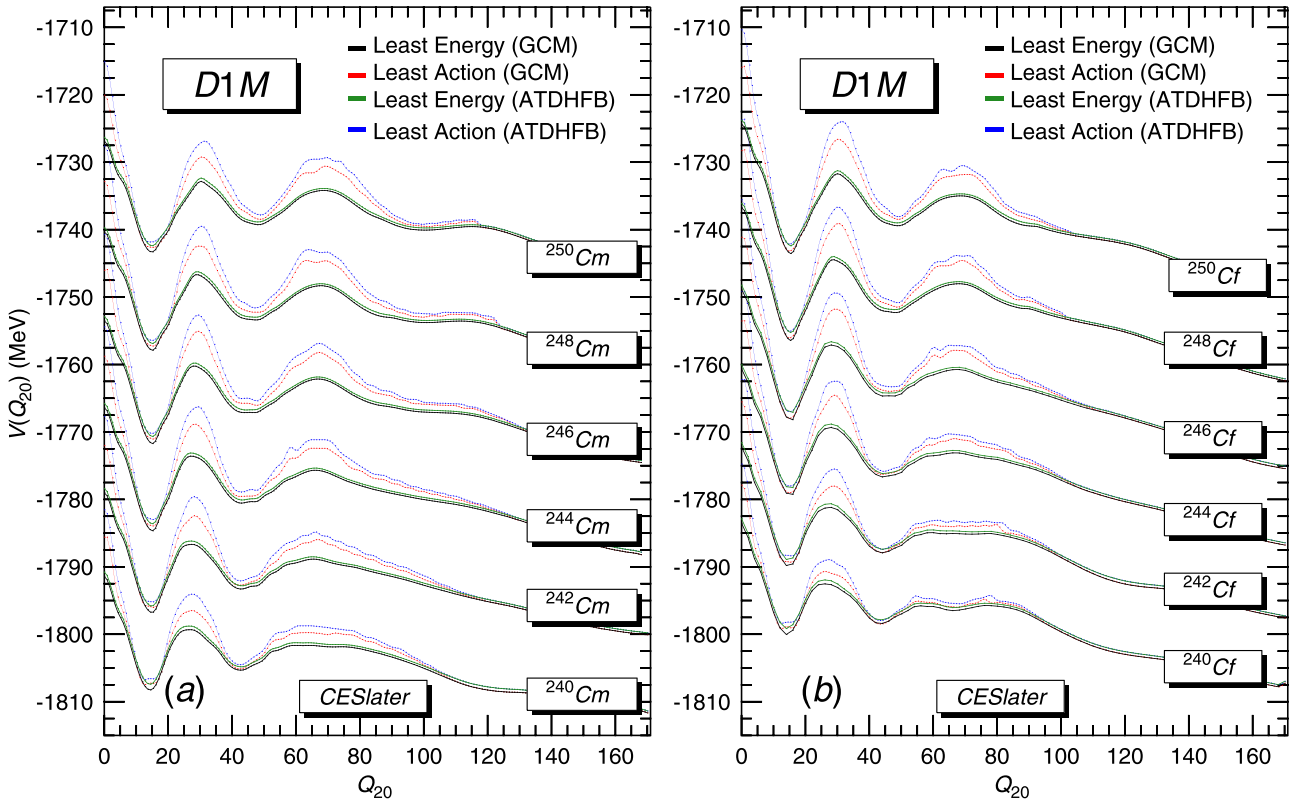

FIG. 5. The CESlater *least action* (LA) collective potentials $V(Q_{20})$ (5) obtained for the nuclei $^{240-250}$Cm and $^{240-250}$Cf, within the GCM and ATDHFB schemes, are plotted in panels (a) and (b), as functions of the quadrupole moment Q_{20}. The CESlater *least energy* (LE) collective potentials are also included in the plots. The paths have been successively shifted by 25 MeV in order to accommodate them in a single plot. Results have been obtained with the parametrization D1M of the Gogny-EDF. For more details, see the main text.

minima are $\mathcal{S}^{\min}_{\mathrm{GCM,CEE}}(Q_{20}=28b)=6.76\times10^{-3}\hbar$ and $\mathcal{S}^{\min}_{\mathrm{ATD,CEE}}(Q_{20}=28b)=7.45\times10^{-3}\hbar$ and they correspond to $\langle\Delta\hat{N}^2\rangle=43$ and 46.

The quenching of the GCM and ATDHFB integrand $\mathcal{S}(Q_{20})$, leads to a reduction of the corresponding actions that appear in the exponential of the spontaneous fission half-lives (2). Thus, the impact on the t_{SF} values is exponential in character. We have computed the CESlater and CEE LA t_{SF} values using the GCM and ATDHFB inertias. For $E_0=0.5$ MeV, the values obtained at the CESlater and CEE levels are given in Table II. These values should be compared with the corresponding LE lifetimes as well as with the experimental value [52] for ^{248}Cf. From the t_{SF} results for ^{248}Cf given in Table II one can conclude the following:

(i) Both at the CESlater and CEE levels, the reductions in the LA GCM and ATDHFB spontaneous fission half-lives bring them closer to the experimental value [52].
(ii) The differences in the predicted LE t_{SF} values arising from the use of GCM and/or ATDHFB masses are significantly reduced within the LA scheme both at the CESlater and CEE levels.
(iii) Within the LE scheme, regardless of the employed GCM and/or ATDHFB mass, the Coulomb antipairing effect leads to CEE spontaneous fission half-lives much larger than those obtained at the CESlater level. However, such discrepancy is cured, to a large extent, within the dynamic description, i.e., the LA scheme provides, regardless of the employed collective mass, CESlater and CEE t_{SF} values, which are essentially of the same quality.

B. Systematic of fission paths and spontaneous fission half-lives in $^{240-250}$Cm and $^{240-250}$Cf

The CESlater LA collective potentials $V(Q_{20})$ (5) obtained for the nuclei $^{240-250}$Cm and $^{240-250}$Cf, within the GCM and ATDHFB schemes, are plotted in Figs. 5(a) and 5(b) as functions of the quadrupole moment Q_{20}. The corresponding CEE LA collective potentials are depicted in Figs. 6(a) and 6(b). The CESlater and CEE LE collective potentials are also included in the plots. The paths have been successively shifted by 25 MeV in order to accommodate them in the plots. We have followed the same methodology described in Sec. III A for ^{248}Cf to compute the LA and LE collective potentials shown in the figures.

The reflection symmetric absolute minima of the CESlater LA and LE paths, shown in Fig. 5, for Cm and Cf isotopes correspond to $Q_{20}\approx14$–16 b. The fission isomers at $Q_{20}\approx42$–52 b are separated from the ground state by the inner barriers, the top of which are located at $Q_{20}\approx24$–34 b.

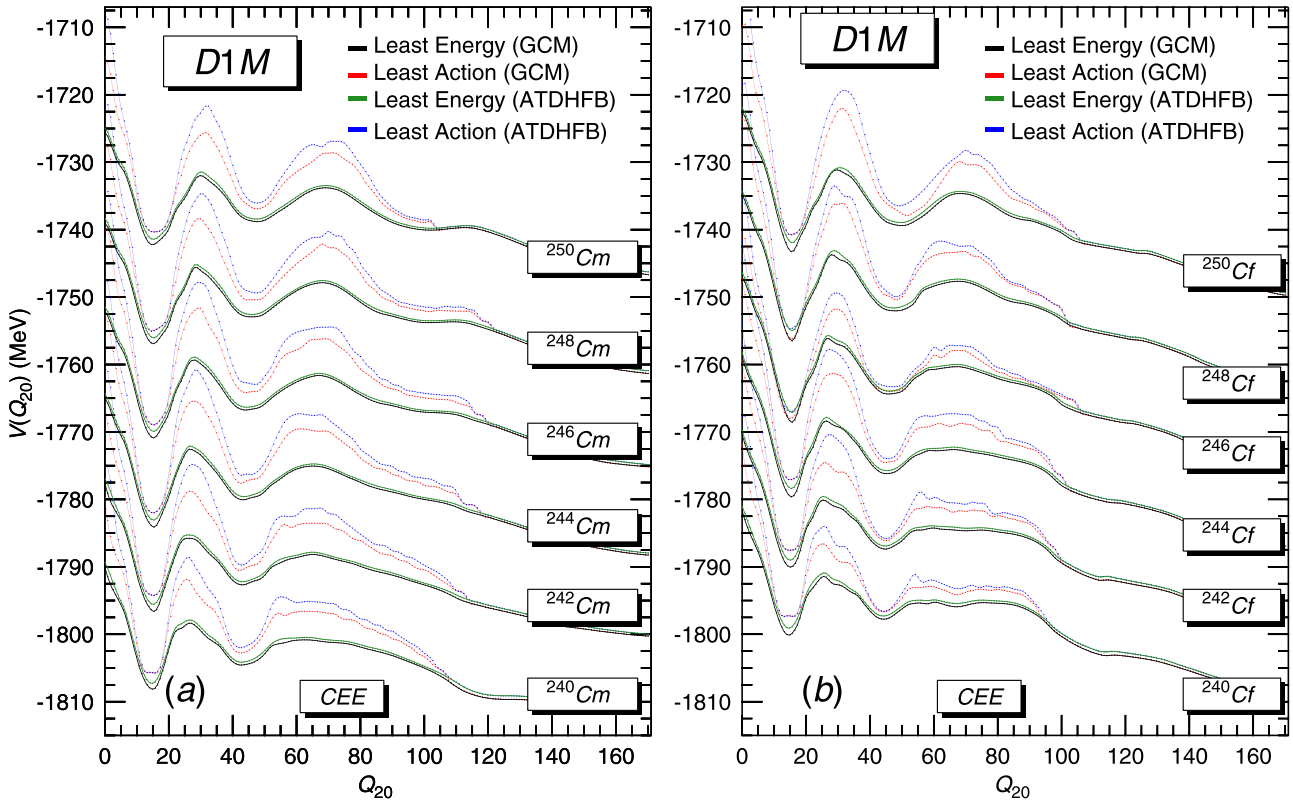

FIG. 6. The CEE *least action* (LA) collective potentials $V(Q_{20})$ (5) obtained for the nuclei $^{240–250}$Cm and $^{240–250}$Cf, within the GCM and ATDHFB schemes, are plotted in panels (a) and (b) as functions of the quadrupole moment Q_{20}. The CEE *least energy* (LE) collective potentials are also included in the plots. The paths have been successively shifted by 25 MeV in order to accommodate them in a single plot. Results have been obtained with the parametrization D1M of the Gogny-EDF. For more details, see the main text.

Octupole correlations play a significant role for quadrupole deformations $Q_{20} \geqslant 56$–62 b and affect the height of the outer barriers, the top of which are located at $Q_{20} \approx 54$–70 b. Similar results hold for the CEE LA and LE paths in Fig. 6. Both at the CESlater and CEE levels, the most pronounced differences between the LE and LA paths are found around the spherical configurations as well as around the top of the inner and outer barriers.

The CESlater and CEE heights B_I and B_{II} of the inner and outer barriers obtained, within the LE and LA GCM and ATDHFB schemes, for $^{240–250}$Cm are plotted in Figs. 7(a) and 7(b) as illustrative examples. For the nuclei $^{240–250}$Cf, the barrier heights display similar trends as functions of A and, therefore, they are not shown in the plots. As can be seen from the figure, the CESlater and CEE LA inner and outer barrier heights are larger than the LE ones. Larger dynamic barrier heights have already been predicted in Gogny-CSlater LA calculations [40,41]. The trends observed in Figs. 5–7 also agree well with previous LA calculations (see, for example, Ref. [50]). As already discussed in Sec. III A [see Figs. 3(a) and 3(d)], this is a consequence of the fact that, for the Q_{20} configurations corresponding to the top of these barriers, the energies increase almost quadratically as functions of $\langle \Delta \hat{N}^2 \rangle$.

However, caution must be taken in connecting the height of fission barriers and spontaneous fission half-lives (see, below). First, fission barriers are not physical observables but inferred (specially LE barrier heights) from cross sections under certain model assumptions (see Ref. [60] and references therein). Second, for a given nucleus the probability to penetrate the fission barrier depends on several other ingredients (for example, shape and width of the barrier) and cannot be solely determined by the barrier height. Third, the behavior and size of the collective inertias also play a key role. Obviously, models employing simpler forms of the collective inertias without pairing dependencies cannot take into account such effects. However, as already shown above and in previous studies [40,41,50], within microscopic mean-field approximations, the increase of the LA barriers, as compared with the LE ones, comes together with a dynamic reduction in the corresponding collective inertias and this leads to a minimum of the action for those Q_{20}-constrained configurations.

The CESlater and CEE spontaneous fission half-lives predicted within the LA GCM and ATDHFB schemes for the isotopes $^{240–250}$Cm are depicted as functions of mass number A in Figs. 8(a) and 8(b). The t_{SF} values obtained for $^{240–250}$Cf are plotted in Figs. 8(c) and 8(d). Calculations have been carried out with $E_0 = 0.5$ MeV. Results corresponding to the LE GCM and ATDHFB schemes are also included in the plots. The experimental t_{SF} values are taken from Ref. [52].

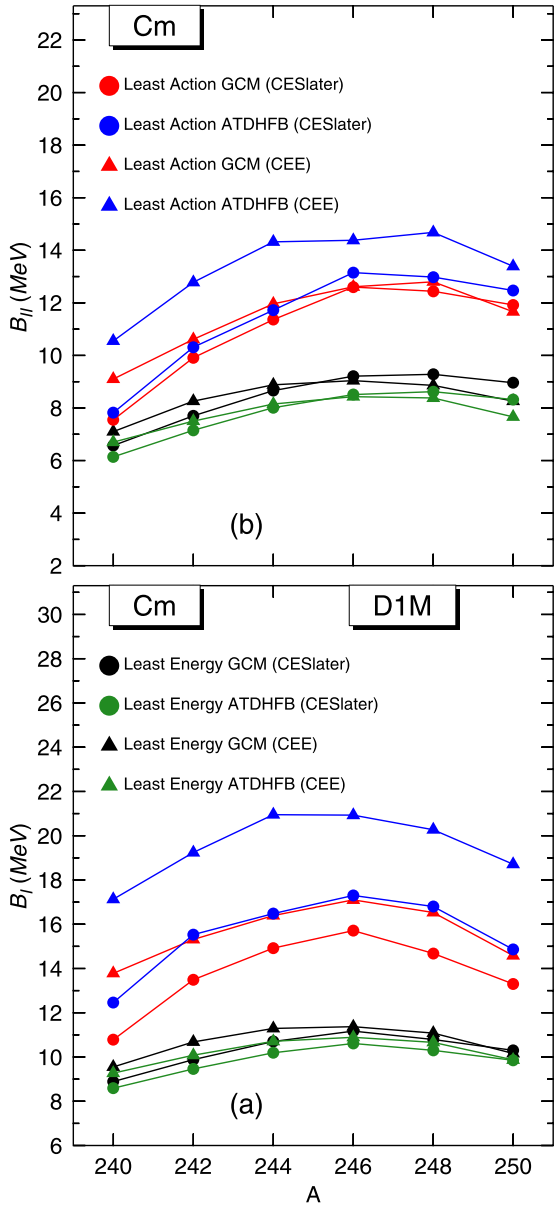

FIG. 7. The CESlater and CEE heights B_I and B_{II} (in MeV) of the inner and outer barriers obtained, within the *least energy* (LE) and *least action* (LA) GCM and ATDHFB schemes, for $^{240-250}$Cm are plotted in panels (a) and (b) as functions of mass number A. The results have been obtained with the Gogny-D1M EDF. For details, see the main text.

On the one hand, both the CESlater and CEE LE approximations already account qualitatively for the experimental trends observed in the spontaneous fission half-lives of the nuclei $^{240-250}$Cm and $^{240-250}$Cf as functions of mass number A. Nevertheless, the LE approximations overestimate the experimental $t_{\rm SF}$ values considerably, especially at the CEE level due to the Coulomb antipairing effect. On the other hand, the LA approaches provide, via larger dynamic pairing correlations, a severe reduction in the predicted GCM and/or ATDHFB $t_{\rm SF}$ values that brings them closer to the experiment [52]. For example, in the case of ^{244}Cm, we have obtained the CESlater (CEE) LE GCM and ATDHFB values $\log_{10} t^{\rm GCM}_{\rm SF,LE} = 20.60$ (34.01) and $\log_{10} t^{\rm ATDHFB}_{\rm SF,LE} = 25.92$ (45.36). It is rewarding to notice that the corresponding CESlater (CEE) LA GCM and ATDHFB values $\log_{10} t^{\rm GCM}_{\rm SF,LE} = 13.53$ (15.22) and $\log_{10} t^{\rm ATDHFB}_{\rm SF,LE} = 15.61$ (17.97) compare much better with the experimental spontaneous fission half-life for this nucleus (see Fig. 8 and Ref. [52]).

Moreover, the pronounced differences observed in Fig. 8 between the LE $t_{\rm SF}$ values computed using the GCM and/or ATDHFB inertias [4], with the ATDHFB results being larger than the GCM ones, are significantly reduced within the LA scheme [41]. For example, in the case of ^{244}Cm, one obtains the CESlater (CEE) values $\log_{10}(t^{\rm ATDHFB}_{\rm SF,LE}/t^{\rm GCM}_{\rm SF,LE}) = 5.32$ (11.35) and $\log_{10}(t^{\rm ATDHFB}_{\rm SF,LA}/t^{\rm GCM}_{\rm SF,LA}) = 2.08$ (2.75). Note that the reduction in those differences is even more pronounced at the CEE level.

Last but not least, the deficiencies introduced in the CEE LE approach by the Coulomb antipairing effect (this effect cannot be properly balanced by static pairing correlations [36]) are, at least for the studied nuclei, cured to a large extent within the considered LA scheme, where beyond-mean-field pairing correlations play a key role when the action is written in terms of pairing degrees of freedom. In fact, as can be seen from Fig. 8, regardless of the GCM and/or ATDHFB mass employed, the CESlater and CEE LA $t_{\rm SF}$ values are essentially of the same quality.

IV. CONCLUSIONS

In this paper, we have examined the role of dynamic pairing correlations for a selected set of Cm and Cf isotopes using the CESlater LA approximation. Within this context, as in previous studies [40,41], HFB(CESlater) calculations have been performed treating the Coulomb exchange term in the Slater approximation while Coulomb and spin-orbit antipairing have been neglected. The impact of Coulomb antipairing and exact Coulomb exchange effects on the LA calculations has also been studied. Calculations have been carried out including all the direct, exchange and pairing contributions coming from the Gogny-D1M EDF and the Coulomb potential [HFB(CEE)]. Constrains on the quadrupole $\hat{Q}_{20}$ and the (total) particle number fluctuation $\Delta\hat{N}^2$ operators have been employed to obtain the LE and LA fission paths. However, it should also be kept in mind that octupolarity is allowed to be broken at any stage of the calculations. The particle number fluctuation $\langle\Delta\hat{N}^2\rangle$ has been identified as a key degree of freedom for the minimization of the WKB action. For the studied nuclei it has been shown that, as in previous CESlater calculations [41], the parabolic increase of the energies as functions of $\langle\Delta\hat{N}^2\rangle$ together with the reduction of the collective GCM and/or ATDHFB masses lead to a minimum of the WKB action at a $\langle\Delta\hat{N}^2\rangle$ value significantly larger than the self-consistent one. This behavior is also present in the LA scheme at the CEE level. As a result, both the CESlater and CEE LA paths exhibit pronounced differences, as compared with the LE paths, around the spherical configurations as well as around the top of the inner and outer barriers for all the studied nuclei. Moreover, it has been shown that both at the CESlater and CEE levels the LA scheme provides, via larger dynamic pairing correlations, a severe reduction in the predicted GCM and/or ATDHFB $t_{\rm SF}$ values that brings them

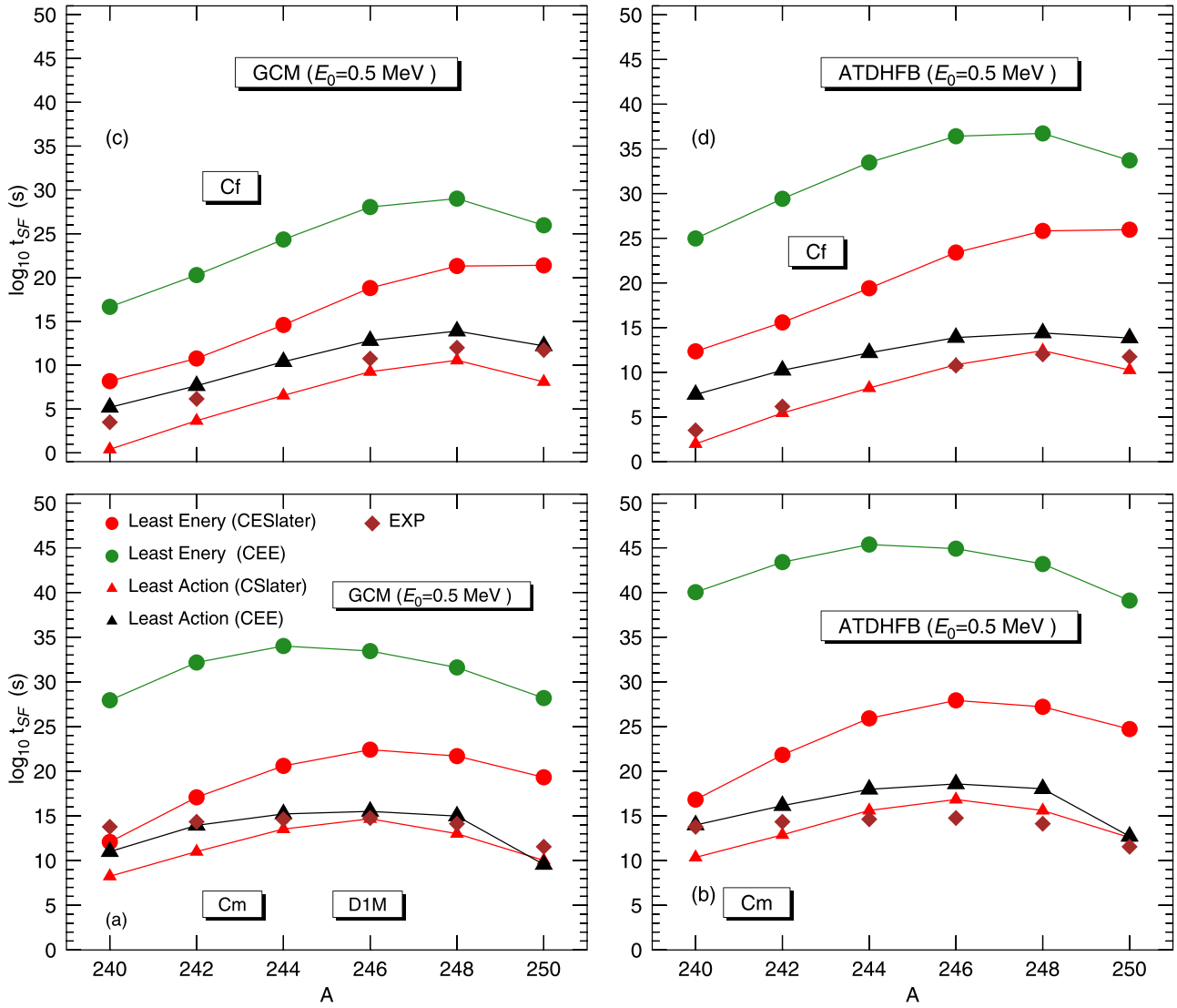

FIG. 8. The CESlater and CEE spontaneous fission half-lives predicted within the *least action* (LA) GCM and ATDHFB schemes for the isotopes $^{240-250}$Cm are depicted as functions of mass number A in panels (a) and (b). The t_{SF} values obtained for $^{240-250}$Cf are plotted in panels (c) and (d). Calculations have been carried out with $E_0 = 0.5$ MeV. Results corresponding to the *least energy* (LE) GCM and ATDHFB schemes are also included in the plot. The experimental t_{SF} values are taken from Ref. [52].

closer to the experiment. The pronounced differences between the LE t_{SF} values computed using the GCM and/or ATDHFB inertias are also significantly reduced within the LA scheme. Furthermore, it has been shown that the strong impact of Coulomb antipairing in the CEE LE approach gets reduced to a large extent within the LA scheme. As a consequence, both CESlater and CEE LA t_{SF} values are essentially of the same quality.

ACKNOWLEDGMENTS

The work of R.R. was supported within the framework of the (distinguished researcher) María Zambrano Program, Seville University. The work of L.M.R. was supported by Spanish Agencia Estatal de Investigacion (AEI) of the Ministry of Science and Innovation under Grant No. PID2021-127890NB-I00.

[1] N. Schunck and L. M. Robledo, Rep. Prog. Phys. **79**, 116301 (2016).
[2] H. J. Krappe and K. Pomorski, *Lecture Notes in Physics* (Springer Verlag, Berlin, Heidelberg, 2012), Vol. 838.
[3] P. Ring and P. Schuck, *The Nuclear Many-Body Problem* (Springer, Berlin, 1980).
[4] R. Rodríguez-Guzmán and L. M. Robledo, Phys. Rev. C **89**, 054310 (2014).
[5] M. Warda and J. L. Egido, Phys. Rev. C **86**, 014322 (2012).
[6] J. F. Berger, M. Girod, and D. Gogny, Nucl. Phys. A **428**, 23 (1984).

[7] J.-P. Delaroche, M. Girod, H. Goutte, and J. Libert, Nucl. Phys. A **771**, 103 (2006).
[8] S. Perez-Martin and L. M. Robledo, Int. J. Mod. Phys. E **18**, 788 (2009).
[9] N. Dubray, H. Goutte, and J.-P. Delaroche, Phys. Rev. C **77**, 014310 (2008).
[10] V. Martin and L. M. Robledo, Int. J. Mod. Phys. E **18**, 861 (2009).
[11] W. Younes and D. Gogny, Phys. Rev. C **80**, 054313 (2009).
[12] M. Warda, J. L. Egido, L. M. Robledo, and K. Pomorski, Phys. Rev. C **66**, 014310 (2002).
[13] J. L. Egido and L. M. Robledo, Phys. Rev. Lett. **85**, 1198 (2000).
[14] R. Rodríguez-Guzmán, Y. M. Humadi, and L. M. Robledo, Eur. Phys. J. A **56**, 43 (2020).
[15] N. Nikolov, N. Schunck, W. Nazarewicz, M. Bender, and J. Pei, Phys. Rev. C **83**, 034305 (2011).
[16] J. D. McDonnell, W. Nazarewicz, and J. A. Sheikh, Phys. Rev. C **87**, 054327 (2013).
[17] J. Erler, K. Langanke, H. P. Loens, G. Martínez-Pinedo, and P.-G. Reinhard, Phys. Rev. C **85**, 025802 (2012).
[18] A. Staszczak, A. Baran, and W. Nazarewicz, Phys. Rev. C **87**, 024320 (2013).
[19] A. Baran, K. Pomorski, A. Lukasiak, and A. Sobiczewski, Nucl. Phys. A **361**, 83 (1981).
[20] M. Baldo, L. M. Robledo, P. Schuck, and X. Viñas, Phys. Rev. C **87**, 064305 (2013).
[21] S. A. Giuliani and L. M. Robledo, Phys. Rev. C **88**, 054325 (2013).
[22] S. A. Giuliani, G. Martnez-Pinedo, and L. M. Robledo, Phys. Rev. C **97**, 034323 (2018).
[23] H. Abusara, A. V. Afanasjev, and P. Ring, Phys. Rev. C **82**, 044303 (2010).
[24] H. Abusara, A. V. Afanasjev, and P. Ring, Phys. Rev. C **85**, 024314 (2012).
[25] B.-N. Lu, E.-G. Zhao, and S.-G. Zhou, Phys. Rev. C **85**, 011301(R) (2012).
[26] S. Karatzikos, A. V. Afanasjev, G. A. Lalazissis, and P. Ring, Phys. Lett. B **689**, 72 (2010).
[27] M. Bender, K. Rutz, P.-G. Reinhard, J. A. Maruhn, and W. Greiner, Phys. Rev. C **58**, 2126 (1998).
[28] Z. Shi, A. V. Afanasjev, Z. P. Li, and J. Meng, Phys. Rev. C **99**, 064316 (2019).
[29] A. Taninah, S. E. Agbemava, and A. V. Afanasjev, Phys. Rev. C **102**, 054330 (2020).
[30] R. Rodríguez-Guzmán and L. M. Robledo, Eur. Phys. J. A **50**, 142 (2014).
[31] R. Rodríguez-Guzmán and L. M. Robledo, Eur. Phys. J. A **52**, 12 (2016).
[32] R. Rodríguez-Guzmán and L. M. Robledo, Eur. Phys. J. A **52**, 348 (2016).
[33] R. Rodríguez-Guzmán and L. M. Robledo, Eur. Phys. J. A **53**, 245 (2017).
[34] S. Pérez-Martín and L. M. Robledo, Phys. Rev. C **78**, 014304 (2008).
[35] R. Bernard, S. A. Giuliani, and L. M. Robledo, Phys. Rev. C **99**, 064301 (2019).
[36] R. Rodríguez-Guzmán and L. M. Robledo, Phys. Rev. C **106**, 024335 (2022).
[37] J. A. Sheikh, J. Dobaczewski, P. Ring, L. M. Robledo and C. Yannouleas, J. Phys. G **48**, 123001 (2021).
[38] C. Titin-Schnaider and Ph. Quentin, Phys. Lett. B **49**, 213 (1974).
[39] J. Sadhukhan, K. Mazurek, A. Baran, J. Dobaczewski, W. Nazarewicz, and J. A. Sheikh, Phys. Rev. C **88**, 064314 (2013).
[40] S. A. Giuliani, L. M. Robledo, and R. Rodríguez-Guzmán, Phys. Rev. C **90**, 054311 (2014).
[41] R. Rodríguez-Guzmán and L. M. Robledo, Phys. Rev. C **98**, 034308 (2018).
[42] M. Brack, J. Damgaard, A. S. Jensen, H. C. Pauli, V. M. Strutinsky, and C. Y. Wong, Rev. Mod. Phys. **44**, 320 (1972).
[43] G. Bertsch and H. Flocard, Phys. Rev. C **43**, 2200 (1991).
[44] M. Urin and D. Zaretsky, Nucl. Phys. **75**, 101 (1966).
[45] K. Pomorski, Int. J. Mod. Phys. E **16**, 237 (2007).
[46] A. Staszczak, S. Pilat, and K. Pomorski, Nucl. Phys. A **504**, 589 (1989).
[47] J. Sadhukhan, W. Nazarewicz, and N. Schunck, Phys. Rev. C **93**, 011304(R) (2016).
[48] J. Zhao, B.-N. Lu, T. Niksic, D. Vretenar, and S.-G. Zhou, Phys. Rev. C **93**, 044315 (2016).
[49] L. G. Moretto and R. P. Babinet, Phys. Lett. B **49**, 147 (1974).
[50] A. Staszczak, A. Baran, K. Pomorski, and K. Böning, Phys. Lett. B **161**, 227 (1985).
[51] J. Sadhukhan, J. Dobaczewski, W. Nazarewicz, J. A. Sheikh, and A. Baran, Phys. Rev. C **90**, 061304(R) (2014).
[52] N. E. Holden and D. C. Hoffman, Pure Appl. Chem. **72**, 1525 (2000).
[53] T. Lesinski, T. Duguet, K. Bennaceur, and J. Meyer, Eur. Phys. J. A **40**, 121 (2009).
[54] H. Nakada and M. Yamagami, Phys. Rev. C **83**, 031302(R) (2011).
[55] S. Goriely, S. Hilaire, M. Girod, and S. Péru, Phys. Rev. Lett. **102**, 242501 (2009).
[56] C. Gonzalez-Boquera, M. Centelles, X. Vinas, and L. M. Robledo, Phys. Lett. B **779**, 195 (2018).
[57] L. M. Robledo and G. F. Bertsch, Phys. Rev. C **84**, 014312 (2011).
[58] J. L. Egido and L. M. Robledo, Lect. Notes Phys. **641**, 269 (2004).
[59] R. Rodríguez-Guzmán, J. L. Egido, and L. M. Robledo, Nucl. Phys. A **709**, 201 (2002).
[60] G. F. Bertsch, W. Loveland, W. Nazarewicz, and P. Talou, J. Phys. G **42**, 077001 (2015).